Available online at www.sciencedirect.com

ScienceDirect

journal homepage: www.elsevier.com/locate/he

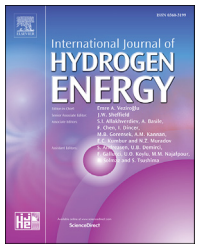

MWCNTs and Cu_2O sensitized Ti–Fe_2O_3 photoanode for improved water splitting performance

Anuradha Verma [a], *Anupam Srivastav* [a], *Shailja Sharma* [a], *Pavan Badami* [c], *Vibha Rani Satsangi* [b], *Rohit Shrivastav* [a], *Arunachala M. Kannan* [c], *Devesh Kumar Avasthi* [d], *Sahab Dass* [a,*]

[a] *Department of Chemistry, Dayalbagh Educational Institute, Dayalbagh, Agra 282005, India*
[b] *Department of Physics & Computer Science, Dayalbagh Educational Institute, Dayalbagh, Agra 282005, India*
[c] *Fuel Cell Research Laboratory, The Polytechnic School, Ira A. Fulton Schools of Engineering, Arizona State University, Mesa, AZ 85212, USA*
[d] *Amity University, Noida 201313, India*

ARTICLE INFO

Article history:
Received 14 November 2017
Received in revised form
28 January 2018
Accepted 31 January 2018
Available online 2 March 2018

Keywords:
Multi-walled carbon nano tubes
Copper oxide
Heterojunction
Photoelectrochemical activity
Hydrogen generation

ABSTRACT

Fe_2O_3 and Cu_2O, both earth abundant materials are used in functionalizing Ti doped Fe_2O_3 photoanodes with Cu_2O and MWCNTs for improving photoelectrochemical performance for hydrogen generation. Pristine Ti doped Fe_2O_3 are fabricated by spray pyrolysis deposition method on the conducting ITO coated glass substrate. Two different modifications are adopted to improve the photoelectrochemical performance of pristine sample by subsequent deposition of multi walled carbon nano tubes (MWCNTs) alone and also in combination with Cu_2O. Better photoresponse in modified samples is attributed to increase in conductivity and promotion of electron transport to Fe_2O_3 layer due to presence of MWCNTs while formation of heterojunction also promotes charge transfer kinetics by effective separation of charge carriers. Offering high photocurrent density of 5.17 mA cm^{-2} at 1 V vs SCE, high open circuit voltage (V_{oc}), least resistance, higher negative flat band potential (V_{fb}), Ti–Fe_2O_3/(MWCNTs + Cu_2O), emerges as the most photoactive sample. High applied bias photon to current conversion efficiency (*ABPE*) value of 4.6% is obtained for the modified sample against 0.07% ABPE for Ti–Fe_2O_3 photoanodes.

Introduction

Hydrogen is clean, sustainable and high energy density fuel. In the present scenario, hydrogen production is mainly based on the techniques which release gases like carbon dioxide contributing to global warming [1,2]. The production of hydrogen by the photoelectrochemical (PEC) water splitting is one of the efficient ways to fulfill the growing energy demand [3]. The PEC water splitting technology potentially provides a new insight to fulfill energy demands as it is based on solar energy and water, both of which are plentiful on earth. The

* *Corresponding author.*
E-mail address: drsahabdas@gmail.com (S. Dass).
https://doi.org/10.1016/j.ijhydene.2018.01.204

development of PEC technology involves making suitable light harvesting material having following properties viz. photochemical stability, corrosion resistance, straddling band edge positions, ability to absorb visible portion of sunlight, low rate of recombination to yield high life time of charge carriers and low cost [4–7]. Significant efforts have been made to modify various metal oxide and non-oxide semiconductors to harness solar energy and making them a potential catalyst. Although there are several reports on numerous tactics to improve the PEC performance but the most popular approaches adopted include doping [8–10], heterojunction [11–13], nanostructuring [14–16], quantum dot sensitization [17,18], plasmons [19,20] and ion irradiation [21,22].

Hematite (α- Fe_2O_3) is a photoactive material with a high potential to be used as catalyst in PEC water splitting. Besides the appropriate band gap (1.9–2.2 eV) lying in visible region, other captivating characteristics include abundance, low cost, non-toxicity, photochemical stability and non corrosive nature. However, the drawback of using hematite lies in its poor water oxidation reaction kinetics which requires high applied bias for oxygen evolution reaction. The other issues involved are high recombination rate of photoexcited charge carriers, short diffusion length of minority charge carriers and poor electrical conductivity. Doping, formation of heterojunction and nanostructuring have been adopted to aggrandize the performance of hematite [23–25].

Cu_2O, a p-type semiconductor with band gap of 1.9–2.2 eV is yet another attractive metal oxide with more or less similar encouraging properties as that of hematite such as opulence, non toxic nature, ascendable and economical. Hydrogen production is feasible by Cu_2O even without the application of external bias due to its straddling band edges with water redox potential. But the application of Cu_2O as competent material for PEC water splitting is hampered by its susceptibility towards photocorrosion and inadequacy for collection of charge carriers [26–27].

Recent studies on carbon nanotubes (CNTs) suggest that they offer excellent electrical and mechanical properties, large surface area and ability to store electrons and also used as supporter for energy storage and conversion. CNTs render the conduction of photogenerated charge carriers and also increases charge injection and extraction [28–32]. The single walled carbon nano tubes (SWCNTs) can be used as channel for transporting electrons in PEC cell for improved PEC conversion efficiency due to their electron accepting properties has been recently demonstrated [33,34]. D. Das et al. investigated the role of CNTs in addressing the corrosion issues in Co_2P/CNT by acting as conductive support for the easy transportation of electrons [30]. E. Kecsenovity et al. studied the role of CNTs in overcoming instability and corrosion issues in special context to Cu_2O and their study revealed that CNTs help in rapid charge carrier separation and transport and in turn was responsible for higher photocurrent and stability. Long term PEC measurements were performed by Kecsenovity et al. with Cu_2O and CNT/Cu_2O and observed 25% of initial photoactivity was retained by Cu_2O alone while 66% was retained by CNT/Cu_2O. The increased stability of CNT/Cu_2O photocathode was attributed to the introduction of highly conductive nanostructured scaffold [35]. Ternary Ag/TiO_2/CNT photoanode was found to exhibit effective interfacial electron transfer which was attributed to the synergetic effect of Ag nanoparticles and CNTs [36]. Improved visible light photoactivity was found in CNTs/MnO_2–C_3N_4 ternary catalyst. CNTs induces evolution of hydrogen by facilitating electron capture from C_3N_4 and MnO_2 helps in oxygen evolution by the decomposition of hydrogen peroxide and this leads to effective separation of photogenerated electron-hole pairs [37]. CNT/g-C_3N_4 photocatalysts was synthesized by Song et al. and enhanced hydrogen production was observed due to synergistic effect between CNTs and g-C_3N_4. Photoelectrons attracted by the CNTs are rapidly transferred to the catalyst interface which resulted in better charge separation as well as effective use of photoelectrons by g-C_3N_4. The stability of g-C_3N_4 was also improved due to the presence of CNTs [38]. ZnO/MWCNT nanocomposite photoelectrode exhibited five times higher photocurrent density (1.14 mA/cm^2 at 1 V vs. Ag/AgCl) in comparison to bare ZnO (0.24 mA/cm^2 at 1 V vs. Ag/AgCl) and this enhanced response was attributed to the conducting CNT scaffolds which promotes charge collection and transport in the ZnO/MWCNT nanocomposite [39].

Fe_2O_3-CNT composite and Fe_2O_3 photoanode modified with MWCNTs have shown remarkably enhanced PEC water oxidation [40,41]. Liu et al. obtained improved PEC response by incorporating functionalized CNTs in Ti-doped Fe_2O_3 thin films showing improved absorption of visible portion of sunlight, reduced recombination of excitons and fast charge transfer [42]. For water purification, in terms of Rhodamine B degradation, enhanced photocatalytic activity of Fe_2O_3/MWCNTs/RGO composite was demonstrated by Pawar et al. [43]. Li et al. studied Co/Cu_2O nanomaterial based on carbon nano tubes which showed enhanced photocatalytic water splitting property [44].

Besides the modification of Fe_2O_3 and Cu_2O with CNTs, an efficient approach is formation of heterojunction between them owing to Z-scheme band alignment (staggered type). This type of band arrangement is of great importance due to their effective charge separation and transfer. Heterojunction α-Fe_2O_3/Cu_2O composite and Ti–Fe_2O_3/Cu_2O bilayered thin films for photoreduction of CO_2 and PEC water splitting for hydrogen generation respectively has been reported in the recent past. The photostability problem of Cu_2O can also be combated by forming type II band alignment with another semiconducting material [45,46].

Recent reports on hematite reveal that co-doping by Sn and Co resulted in photoelectrochemical response of 1.25 mA/cm^2 at 1.23 V/RHE [47]. Hydrothermally fabricated α-Fe_2O_3/CQDs heterojunction photoanode shows eight time increment in photocurrent density (0.35 mA/cm^2 at 1.23 V/RHE) in comparison to bare hematite [48]. Zhang et al. investigated the effects of Sn precursors on the morphology, surface characteristics and the PEC properties of hematite photoanode and maximum photocurrent achieved was 1.54 mA/cm^2 at 1.23 V/RHE [49].

In the present study, we have designed and developed Ti-doped Fe_2O_3based photoanodes modified with MWCNTs alone and MWCNTs-Cu_2O nanopowder composites. We schematically show here the various approaches taken in this study with the sole aim to improve the performance of α-Fe_2O_3 (Fig. 1). To enhance the electrical conductivity of hematite, Ti was used as dopant and this material was considered as pristine sample. MWCNTs as a layer was deposited over the Ti–

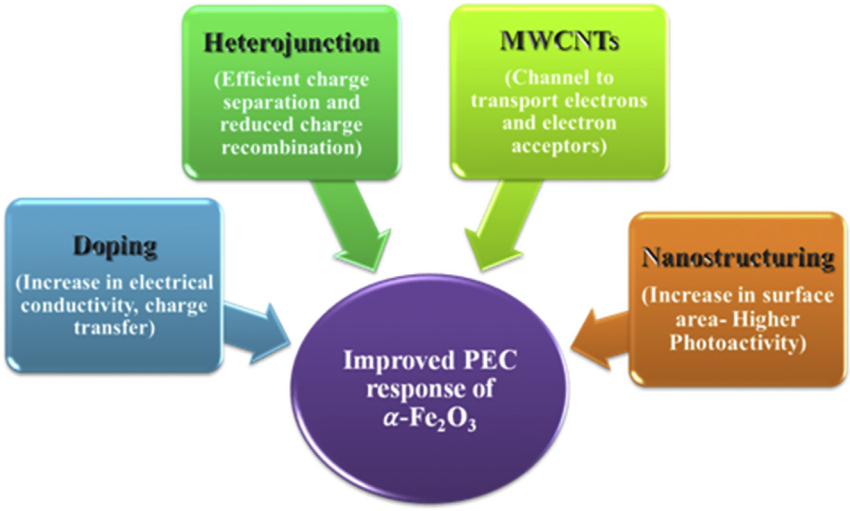

Fig. 1 – Schematic presentation of various strategies adopted in the present study.

Fe_2O_3 thin film to make Ti–Fe_2O_3/MWCNTs photoanode while in other case both MWCNTs and Cu_2O nanopowder suspension was deposited to fabricate the Ti–Fe_2O_3/(MWCNTs + Cu_2O) photoanode. In Ti–Fe_2O_3/(MWCNTs + Cu_2O) system both MWCNTs and formation of heterojunction between hematite and cuprous oxide played an influential role in improving the photoelectrochemical behavior of hematite. In addition to this, nanostructuring is well established way of improving the photoelectrochemical performance with increased surface area and in present case Cu_2O nanopowder with size of 18 nm is assumed to play synergistic role. Multiple factors, therefore, may contribute for excellent PEC performance. Detailed structural, optical and morphological examination of the prepared samples was done along with PEC characterizations. The mechanism proposed for improved PEC properties of Ti–Fe_2O_3/(MWCNTs + Cu_2O) have also been discussed.

Experimental

Photoanode fabrication

The scheme of fabrication of photoanodes on ITO-coated glass substrate is shown in Fig. 2. Thin film of Ti doped (2 at%) Fe_2O_3 was prepared by spray pyrolysis. Iron nitrate nonahydrate ($Fe(NO_3)_3 \cdot 9H_2O$; Sigma Aldrich) and titanium tetrachloride ($TiCl_4$; Sigma Aldrich) were used as precursors without further purification and dissolved in distilled water (solution molarity 0.15 M). The details of the method can be seen from the work reported by the authors previously [20]. A transparent conducting ITO coated glass substrates (coated on one side by Sn-doped indium oxide, resistivity approximately 8 Ω-cm) were used to deposit Ti–Fe_2O_3 thin film and almost one third portion was covered with Al foil which was used later to make electrical contact with Cu wire and conducting Ag paste for PEC measurements. The thickness of Fe_2O_3 layer was around 500 nm and measured using surface profilometer (Alpha Step D-Tencor T-120). Prior to deposition, the ITO substrates were cleaned to remove any dirt and impurity particles. ITO substrates were dipped in mixture of methanol (CH_3OH; Sigma Aldrich) and DM water (Avarice Industries) and kept for ultrasonication for duration of 10 min and then dried in oven.

To modify the materials property two different suspensions were made:

MWCNTs suspension

Optimum concentration (0.2 wt%) of MWCNTs (Aldrich) suspension was made in a mixture of 9:1 ratio of iso-propyl

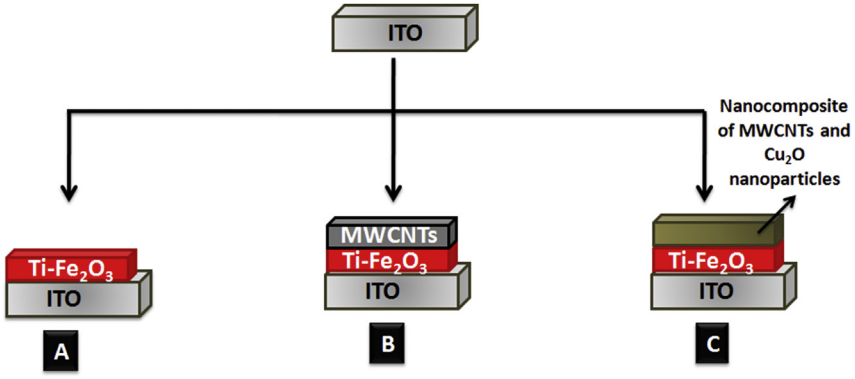

Fig. 2 – Diagrammatic presentation of prepared photoanodes.

alcohol $(CH_3)_2CHOH$, Sigma Aldrich) and Nafion (5 wt%) respectively. The suspension was stirred and sonicated alternatively for 4 h.

Cu_2O and MWCNTs suspension

Cu_2O nanopowder (US Research Nanomaterials) was weighed and dissolved in the suspension detailed above for the preparation of MWCNTs suspension. 16 wt% of Cu_2O nanopowder suspension was made with same amount of MWCNTs. This suspension was alternatively stirred and sonicated continuously for 4 h. Only one concentration which was optimum among 4 wt%, 8 wt%, 16 wt % and 32 wt% is discussed here for simplification and elucidating the effect of MWCNTs alone and together with Cu_2O, although other concentrations were also taken which are not detailed in the present communication.

Over the prepared thin films of Ti–Fe_2O_3 approximately 0.1 mL of suspension as detailed in 2.1.1 and 2.1.2 was coated as 4 different layers by spin coating method at 2500 rpm to get two different configurations 1) Ti doped Fe_2O_3 modified with MWCNTs (*Sample B*) 2) Ti doped Fe_2O_3 modified with (MWCNTs + Cu_2O) (*Sample C*). The films were subsequently sintered at 450 °C for 1 h in an inert Ar atmosphere to avoid oxidation of MWCNTs into CO_2. The acronyms of the resulted samples used in this presentation are given in Table 1.

Physicochemical characterization

The X-ray diffraction of thin films was performed by glancing angle Bruker AXS D8 Advance, X-ray diffractometer using Cu Kα radiation. The samples were scanned from 20° to 60° 2θ range. The morphology of fabricated films was observed by field-emission scanning electron microscopy (FESEM) using Carl Zeiss SUPRA 40VP system. The FESEM fitment MIRA II LMH TESCAN energy-dispersive X-ray (EDX) was used to obtain the elemental map of the sample. The optical absorption spectra of the samples were evaluated from the UV–visible absorbance vs. wavelength data and for measuring absorbance UV-1800, Shimadzu, Japan, Double Beam UV–visible spectrometer was used. To confirm the presence of Cu nanoparticles in Cu_2O nanopowder, the suspension of Cu_2O was made in water with concentration of 10 mg/mL and then the absorbance was recorded using UV–visible spectrometer.

Photoelectrochemical measurements

The synthesized films were converted into the electrodes by making ohmic contact at the uncoated surface using Cu wire and Ag paste. The contact area and the edges were covered with non conducting epoxy resin (Hysole, Singapore). The effective area of illumination was 1 cm^2 (1 cm × 1 cm) and these electrodes were used as working photoanodes in PEC studies.

The PEC measurements were conducted in an electrochemical cell with three-electrode configuration with Pt guaze (Geometric area: 1 cm^2 in area) as counter electrode and saturated calomel electrode (SCE) as the reference electrode. The aqueous NaOH (Merck, pH ~ 13) electrolyte was used for PEC study. The illumination (100 $mWcm^{-2}$) was provided with 150 W Xe-arc lamp. A linear sweep voltammetry (potential range −1 to 1 V vs SCE, scan rate 20 mV/s, under dark and light conditions) to get current-voltage characteristics, Mott-Schottky analysis to get the flat band potential, V_{fb} (under dark condition, potential range −1 to 1 V vs SCE, AC potential frequency of 10 kHz and amplitude of 10 mV), electrochemical impedance spectroscopy to get information about charge transfer resistance from nyquist plot (DC potential of 1 V vs SCE and an AC potential frequency range of 10 kHz to 10 mHz with an amplitude of 10 mV) and chronoamperometry to examine the stability (current-time, at fixed potential of 1 V vs SCE for 1 h) was performed using Electrochemical workstation (Zahner, Germany). The open circuit voltage (V_{oc}) was obtained for photoanodes (under illumination condition) to get the applied bias photon to current conversion efficiency (*ABPE*) using the formula:

$$ABPE\ (\%) = J_{ph}\ (mA/cm^2) \times [1.23 - V_b\ (V)]/P\ (mW/cm^2) \times 100$$

where J_{ph} is photocurrent density, applied bias is V_b (V_{meas}–V_{oc}) and P represents the illumination power intensity where V_{meas} is the applied bias at which photocurrent was measured. The chronoamperometry data was also utilized to calculate the amount of hydrogen gas which was compared with the evolved hydrogen gas volume. The close concord between evolved and calculated hydrogen volume is indicated from Faraday efficiency being close to unity [20].

Table 1 – Description of samples.

S. No.	Sample description	Acronym
1	Ti doped Fe_2O_3	A
2	Ti doped Fe_2O_3 modified with MWCNTs	B
3	Ti doped Fe_2O_3 modified with (MWCNTs + Cu_2O)	C

Results and discussion

Morphology and structure

Fig. 3 shows the measured XRD patterns of the Ti doped Fe_2O_3 (A), Ti doped Fe_2O_3 modified with MWCNTs (B) and Ti doped Fe_2O_3 modified with MWCNTs and Cu_2O (C). The diffraction peak of Fe_2O_3 for sample A can be indexed to (012), (100), (113), (024), (116) and (122) diffractions of rhombohedral hematite (JCPDS card no: 24-0072). No peak of MWCNTs was visible as concentration was below the detection limit of XRD. The prominent diffraction peaks at (111) and (200) are assigned to Cu_2O (cuprite phase) and metallic copper (fcc structure). The peaks at $2\theta = 36.44$ and 42.33° match well with the standard pattern (JCPDS: 78-2076), consistent with the values reported previously by Chen et al. [50] while peaks assigned to cubic phase of Cu were obtained at $2\theta = 43.29$ and 50.43° (JCDPS: 04-0836) and match well with the findings of Su et al. [51] in sample C along with the peaks of hematite.

The metallic Cu peak in XRD confirms its presence as foreign nanoparticles along with Cu_2O nanoparticles. The presence of Cu nanoparticles was further confirmed by

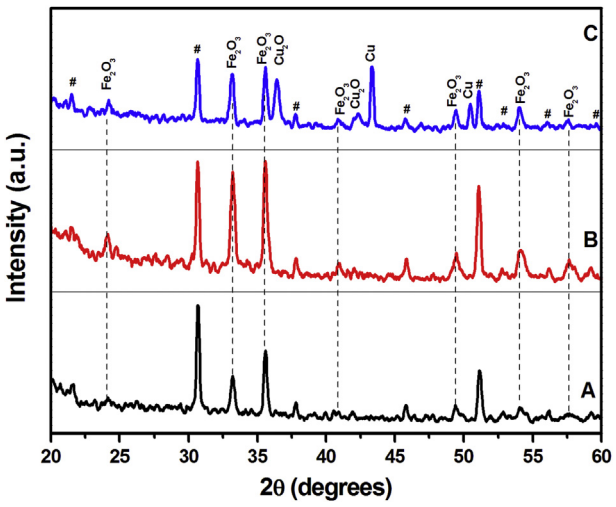

Fig. 3 – XRD pattern of sample A (Ti doped Fe_2O_3), B modified with MWCNTs and C modified with (MWCNTs + Cu_2O).

recording optical absorption spectra discussed in forthcoming section. The average crystallite size of Cu nanoparticles was around 39 nm calculated using Debye Scherrer formula. In addition to diffraction peak of deposited composition in thin films, the peaks indicated with hash tag (#) in Fig. 3 are assigned to underlying ITO coating of glass substrate.

Fig. 4(a–d) shows the top-view FESEM images of fabricated Ti–Fe_2O_3 and heterostructured Ti–Fe_2O_3/(MWCNTs + Cu_2O) and EDX map of sample C. The mesoporous morphology of hematite with uniform deposition at ITO can be seen from Fig. 4 (a) and such kind of morphology has been previously reported [20,52]. Fig. 4 (b) shows the presence of spherical Cu_2O nanoparticles uniformly deposited over the Ti–Fe_2O_3 layer and the size of Cu_2O nanoparticles lies in the range of 18–20 nm. Particle size was calculated using Image-J software and is in close agreement with the size calculated from XRD data using Debye Scherrer's formula with size of 22 nm [53]. The diameter of MWCNTs as revealed from SEM is about 40 nm. The inset in Fig. 4(b) shows the higher resolution image (scale bar: 200 nm). Fig. 4(c–d) illustrates the elemental composition (EDX map) of sample C taken at two different points and confirms the presence of the elements namely 'Fe', 'O', 'Cu', 'C', 'Ti' and 'In'.

Optical response

Illustration of optical absorption spectra is shown in Fig. 5 (a). As can be seen the Ti–Fe_2O_3 (sample A) shows a minimum absorbance with absorption edge at 602 nm while incorporation of MWCNTs and MWCNTs and Cu_2O increases the

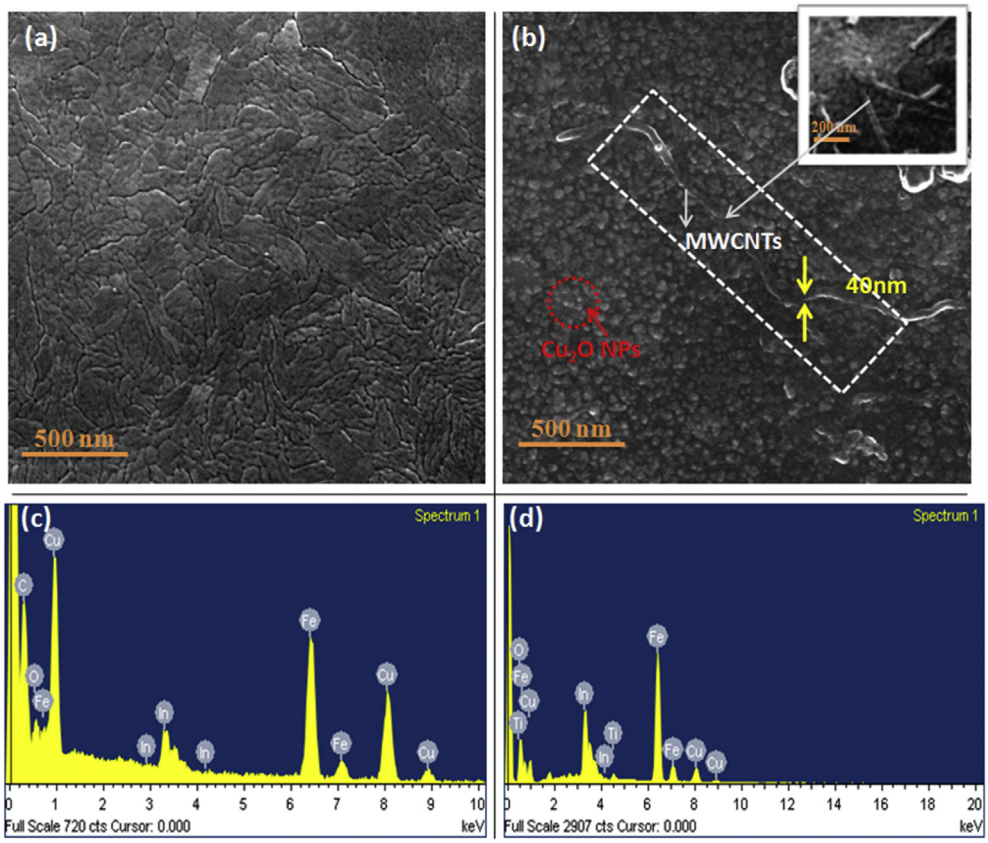

Fig. 4 – (a) FESEM image of Ti–Fe_2O_3 (sample A) (b) FESEM image of sample C showing presence of Cu_2O nanoparticles and MWCNTs (inset is showing the image at higher resolution of 200 nm) (c–d) EDAX map of sample C taken at two different points.

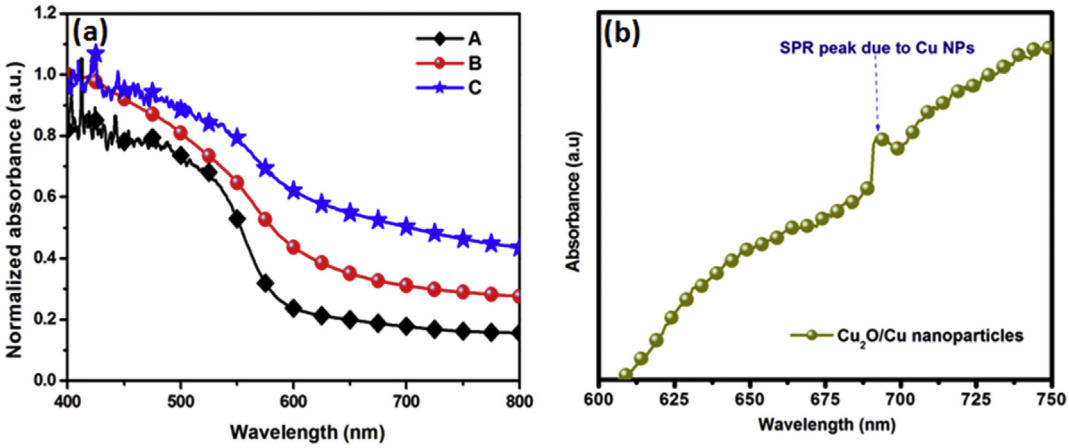

Fig. 5 – (a) Normalized absorbance of sample A, B and C (b) Absorbance of Cu_2O nanopowder showing SPR peak of metallic Cu.

absorbance in whole spectral region. Significant increase in absorbance here is ascribed to the presence of MWCNTs as well as the formation of heterojunction between metal oxides and thus can efficiently harvest the visible portion of sunlight. The increase in visible light absorption due to the MWCNTs has been reported [42].

The presence of Cu nanoparticles was confirmed by XRD pattern as discussed in Section Morphology and structure. To confirm the surface plasmon resonance exhibited by the Cu nanoparticles, absorbance spectra was recorded and is shown in Fig. 5 (b). The absorbance spectra clearly show the characteristic peak at 690 nm. Chan et al. reported LSPR peaks of Cu nanoparticles of different size and also studied the effect of removal of copper oxide species on the LSPR peak. Their study revealed that Cu nanoparticles with size of 40 nm show λ_{max} in the range of 690–710 nm [54]. The SPR peak of Cu nanoparticles in the absorbance spectrum of Sample C subsides (Fig. 5 (a)) due to dominating absorbance of Cu_2O and Fe_2O_3 however overall increase in the absorbance in comparison to other samples is clearly visible that may also be attributed to the presence of plasmonic Cu nanoparticles [20,55].

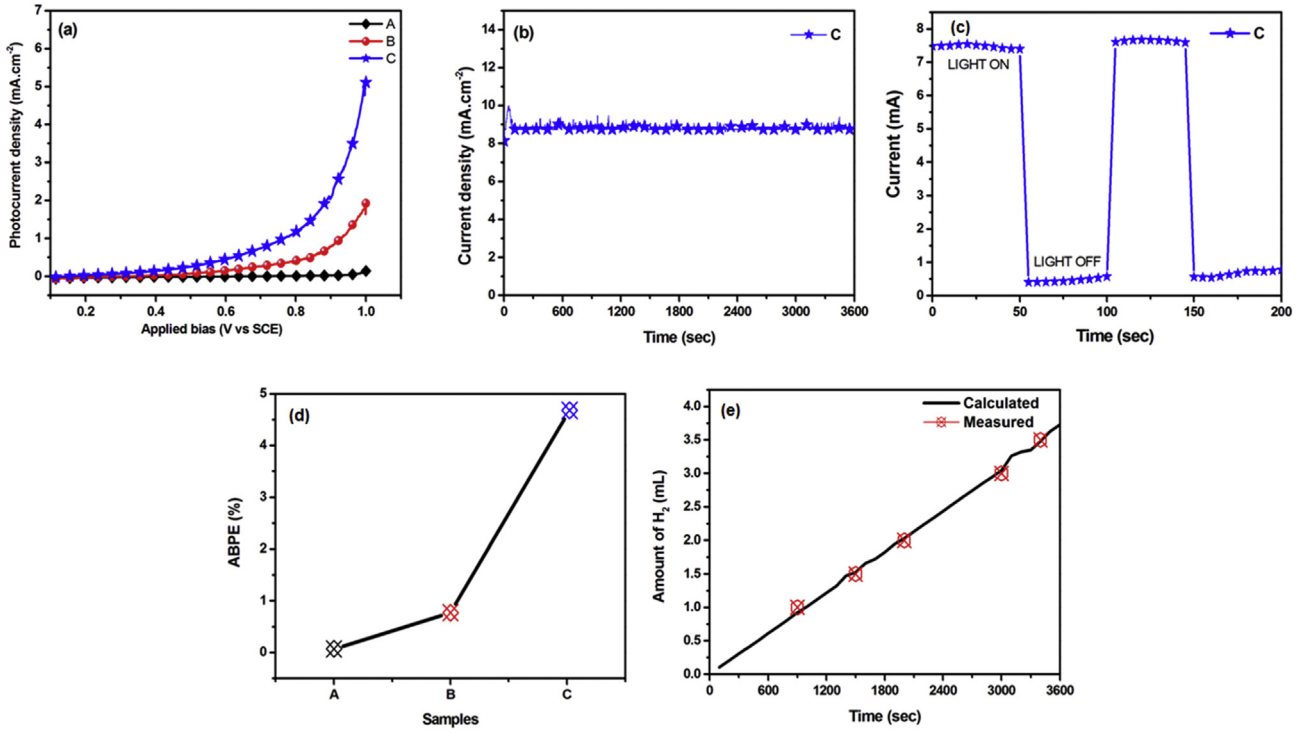

Fig. 6 – (a) Photocurrent density of photoanodes (b–c) Chronoamperometry and Light on-off measurement at applied bias of 1 V vs. SCE for sample C (Ti–Fe_2O_3/(MWCNTs + Cu_2O)) (d) ABPE trend (e) Faraday efficiency for sample C (Ti–Fe_2O_3/(MWCNTs + Cu_2O)).

Photoelectrochemical hydrogen generation

The photoelectrochemical measurements were carried out in three electrodes cell. The comparison of photocurrent density (J_{ph}) of three samples obtained by subtracting their respective dark currents from the light currents is shown in Fig. 6(a). The dark and light current scans of all the samples are given in Supporting Information, Fig. S1. At applied bias of 1 V vs SCE approximately 8 times increase in photocurrent density after was obtained after adding a layer of MWCNTs alone while 32 times increment observed after adding nanocomposite of (MWCNTs + Cu_2O) indicating that sample C has high PEC efficiency. Fig. 6(a) not only illustrates the increase in photocurrent density value but also shows the change in the onset potential. Photocurrent begins to elevate at lower potential in sample C in comparison to A and B. To examine the photostability in aqueous condition, the sample C was subjected to chronoamperometric testing under 1 sun illumination condition at 1 V vs SCE (Fig. 6(b)) for an hour. The stable current under illumination for 1 h confirms the photostability of sample. Chronoamperometric measurements (Fig. 6(b)) show higher current density being recorded under illumination condition only at applied bias of 1 V vs SCE than the J_{ph} vs applied bias plot (Fig. 6(a)) which shows the difference of light and dark current. Effect of light on sample C was checked by light on-off measurements shown in Fig. 6 (c).

To calculate the *ABPE*, the open circuit potential was also measured and the values are reported in Table 2. The high *ABPE* of 4.6% was obtained for sample C which is 6 orders of magnitude higher than the pristine sample. The increase in *ABPE* after each modification can be seen in Fig. 6 (d). The Faradaic efficiency for the sample giving the maximum photoresponse i.e. sample C was measured and is shown in Fig. 6(e). A close compliance between the calculated and evolved H_2 volume is indicated from the Faradaic efficiency being nearly unity suggesting evolution of H_2 and O_2 in 2:1 ratio [20].

The Mott-Schottky analysis was carried out to probe the charge transfer at electrode electrolyte interface and the plots

Table 2 – Photoelectrochemical parameters measured for photoanodes.

Sample	Photocurrent density, J_{ph} (mA.cm^{-2}) at 1 V vs SCE	Open circuit voltage, V_{oc}	Charge transfer resistance (Ohm)	ABPE (%)	Flat band potential, V_{fb}
A	0.16	0.26	55.31	0.07	−0.32
B	1.92	0.39	26.97	1.19	−0.68
C	5.17	0.67	23.62	4.6	−0.84

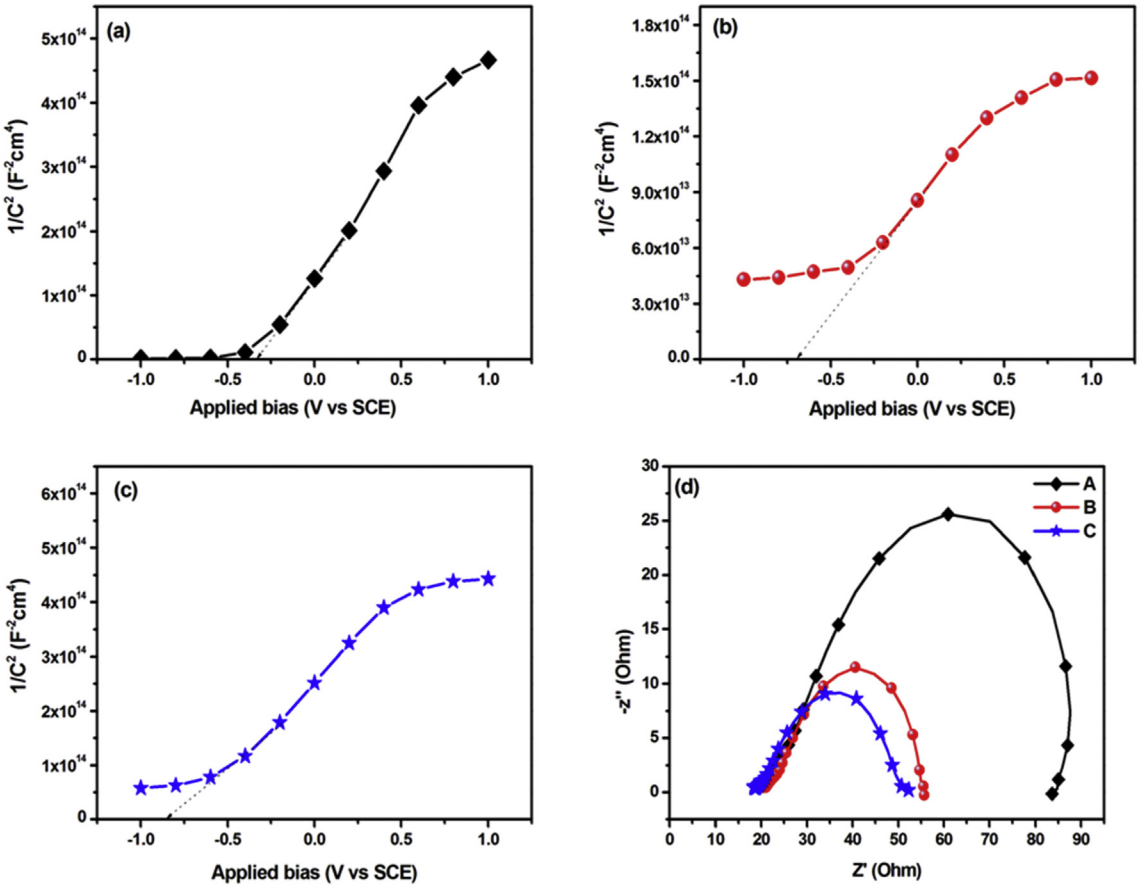

Fig. 7 – (a–c) Mott- Schottky plot and (d) Nyquist plots for sample A, B and C.

are displayed in Fig. 7(a–c). The slope of the curves gives the value of flat band potential which is given in Table 2. A more negative value of flat band potential indicates better charge separation and reduced charge recombination. Interestingly, among the three samples, Ti–Fe_2O_3/(MWCNTs + Cu_2O) sample is showing a negative shift of 0.52 V vs SCE (magnitude only) in comparison to pristine sample, confirming enhanced charge separation and transfer although improvement on the basis of flat band potential values can also be seen for sample B.

To further ensure the improved charge transfer kinetics at electrode electrolyte interface, the samples were subjected to illumination at applied bias of 1 V vs SCE and electrochemical impedance spectroscopy data was collected and is presented here in the form of Nyquist plots in Fig. 7 (d). A smaller diameter of semicircle in case of sample C provides the evidence for reduced charge transfer resistance [21]. In case of sample C, introduction of MWCNTs as well as Cu_2O is favorable for effective charge carrier separation. The experimental data was fitted using EC lab (Zview) software. The fitted plot along with experimental plot and equivalent circuit model (one resistor and two RC circuits) is provided in Supporting Information, Fig. S2. The value of charge transfer resistance at electrode electrolyte interface (R2) was found to be 55.31 Ω, 26.97 Ω and 23.62 Ω respectively for sample A, B and C respectively. The smallest value of charge transfer resistance in sample C confirms the faster charge transfer and lower recombination of photogenerated charge carriers. The decrease in charge transfer resistance also provides further evidence for high J_{ph} in the modified samples and the values are listed in Table 2.

A significantly improved photoelectrochemical response in case of sample C can be attributed to the cumulative effect of multiple factors. The particle size of Cu_2O is small as revealed from SEM and XRD data which reasonably increases the surface area of the film and nanostructuring is beneficial for high PEC activity. Further, to increase the electrical conductivity Ti was added as dopant in Fe_2O_3 sample. The enhancement in optical absorption after introduction of MWCNTs and Cu_2O is also helpful to increase light sensitivity in both sample B and C. The maximum absorption in case of sample C can also be accounted by presence of SPR exhibited by Cu nanoparticles.

The mechanism of charge transfer in staggered type II band alignment for Fe_2O_3 and Cu_2O is shown schematically in Fig. 8 [46]. The position of conduction band (CB) and valence band (VB) for both Cu_2O and Fe_2O_3 are taken from the reported literature [56]. The CB for Cu_2O and Fe_2O_3 lies at −0.2 eV/NHE and 0.5 eV/NHE and VB lies at 1.8 eV/NHE and 2.4 eV/NHE respectively. This type of band arrangement is also helpful in countering the corrosion problem associated with Cu_2O. On illumination electron transfer from conduction band of Cu_2O to the low lying conduction band of Fe_2O_3 may be facilitated directly from Cu_2O or may be shuffled through MWCNTs which is acting as electron collector in Cu_2O matrix. Thus presence of MWCNTs in Cu_2O matrix helps in easy conduction of the electrons. The electrons will finally reach the Pt counter electrode through conducting ITO layer to evolve H_2 and direction of hole movement will be reverse and drift towards the

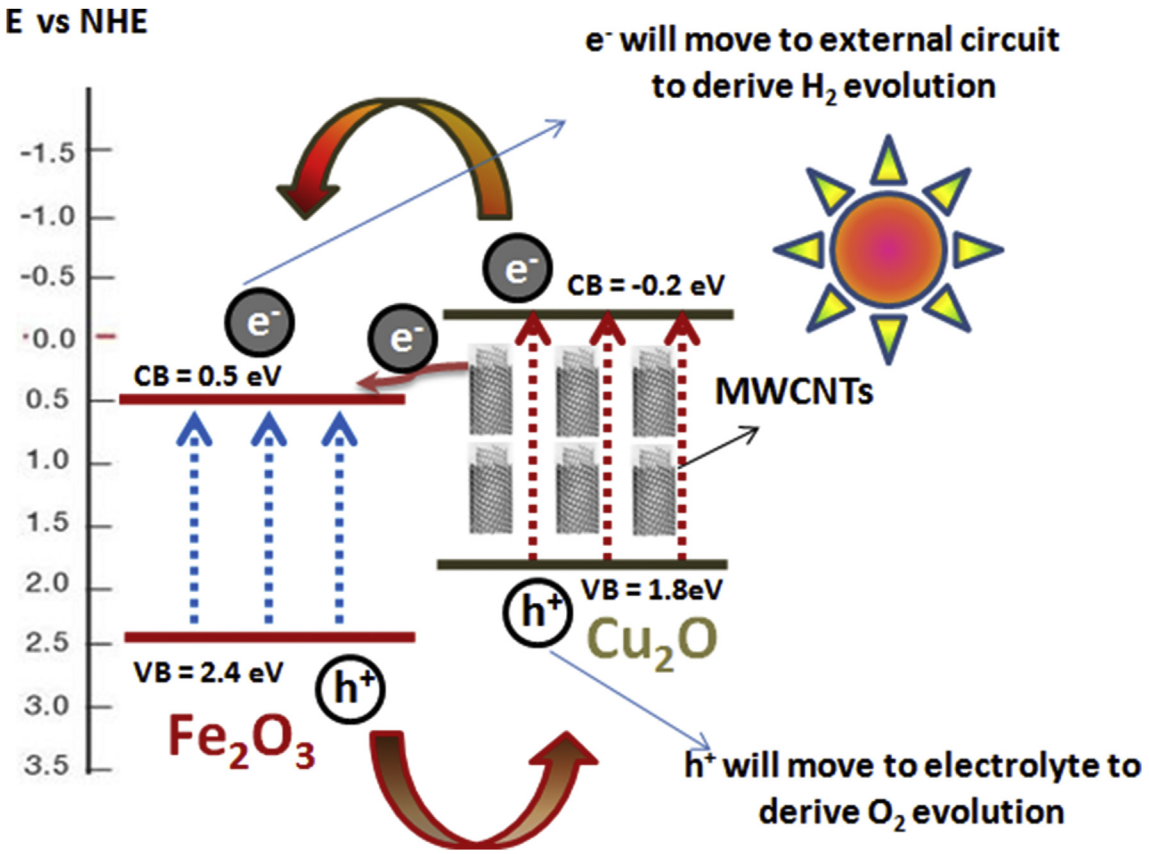

Fig. 8 – Schematic presentation on mechanism for charge transfer.

Table 3 – Comparison of previously reported results based on the materials investigated in the present study.

Semiconductor system investigated	Electrolyte	Light source	Applied bias	Photocurrent density	Reference
Fe_2O_3/MWCNTs composite	1 M NaOH	Solar Simulator (100 mWcm^{-2} AM 1.5 G)	0.4 V vs Ag/AgCl	0.22 mA cm^{-2}	[40]
CNTs and Ti co-doped Fe_2O_3	1 M NaOH	300 W Xe lamp (150 mWcm^{-2})	1.23 V vs RHE	4.5 mA cm^{-2}	[42]
Fe_2O_3/MWCNT/RGO composite	1 M NaOH	Visible light	–	0.495 mA cm^{-2}	[43]
Ti–Fe_2O_3/Cu_2O Heterojunction	0.1 M NaOH	150 W Xe lamp	0.95 V vs SCE	2.6 mA cm^{-2}	[46]
Sample C (Ti–Fe_2O_3)/(MWCNTs + Cu_2O)	0.1 M NaOH	150 W Xe lamp	1.0 V vs SCE	5.1 mA cm^{-2}	***Present study***

photoanode/electrolyte interface for O_2 evolution. On the basis of overall performance of sample C, we infer that several factors are contributing towards enhanced PEC performance. The increase in photoelectrochemical response of Fe_2O_3 photoanodes modified with carbon nano tubes (CNTs) has been previously investigated by various authors while Cu_2O modification with MWCNTs has been reported for photocatalytic hydrogen generation [40,42,43]. The comparison of photoelectrochemical performance of systems including Fe_2O_3, Cu_2O and carbon nano tubes (CNTs) along with the results obtained in present study are summarized in Table 3.

It can be seen that sample C exhibits good performance over the previously reported results which may be attributed to the factors discussed above.

Conclusions

Using earth abundant materials (Ti–$Fe_2O_3$with additional layers of MWCNTs and Cu_2O nanoparticles) photoanodes were designed and developed for photoelectrochemical hydrogen generation. Various photoelectrochemical studies were performed to justify the enhanced photoresponse of Ti–Fe_2O_3/(MWCNTs + Cu_2O) anodes. The stability against photocorrosion was also evaluated by subjecting the photoanode for continuous illumination of 1 h. The Z scheme of electron transfer in this kind of arrangement is also proposed for better separation and conduction of charge carriers and their obstacle-free movement. The high ABPE value for Ti–Fe_2O_3/(MWCNTs + Cu_2O) was attributed to enhanced charge transfer and separation, reduced recombination and decrease in charge transfer resistance. More negative value of flat band potential, low resistance and high open circuit voltage also support the findings. The nanostructured Cu_2O and changes in optical band gap also plays a significant role in improving the PEC performance.

Acknowledgment

Financial support from University Grants Commission, Government of India, through Indo-US 21st Century Knowledge Initiative Project F. No. 194-I/2009(IC) operational between Arizona State University, USA and Dayalbagh Educational Institute, Agra, India, is gratefully acknowledged. AV thanks UGC further for Research Fellowship. Authors thank Dr. Saif Ahmad Khan (IUAC, New Delhi) for SEM and EDX facilities.

Appendix A. Supplementary data

Supplementary data related to this article can be found at https://doi.org/10.1016/j.ijhydene.2018.01.204.

REFERENCES

[1] Kitano M, Hara M. Heterogeneous photocatalytic cleavage of water. J Mater Chem 2010;20(4):627–41.
[2] Lewis NS, Nocera DG. Powering the planet: chemical challenges in solar energy utilization. Proc Natl Acad Sci Unit States Am 2006;103(43):15729–35.
[3] Li Y, Zhang JZ. Hydrogen generation from photoelectrochemical water splitting based on nanomaterials. Laser Photon Rev 2010;4(4):517–28.
[4] Zhu J, Zäch M. Nanostructured materials for photocatalytic hydrogen production. Curr Opin Colloid Interface Sci 2009;14(4):260–9.
[5] Alexander BD, Kulesza PJ, Rutkowska I, Solarska R, Augustynski J. Metal oxide photoanodes for solar hydrogen production. J Mater Chem 2008;18(20):2298–303.
[6] Walter MG, Warren EL, McKone JR, Boettcher SW, Mi Q, Santori EA, et al. Solar water splitting cells. Chem Rev 2010;110(11):6446–73.
[7] Osterloh FE. Inorganic nanostructures for photoelectrochemical and photocatalytic water splitting. Chem Soc Rev 2013;42(6):2294–320.
[8] Ding D, Dong B, Liang J, Zhou H, Pang Y, Ding S. Solvothermal-etching process induced Ti-doped Fe_2O_3 thin film with low turn-on voltage for water splitting. ACS Appl Mater Interfaces 2016;8(37):24573–8.
[9] Arifin K, Kadir HA, Minggu LJ, Daud WRW, Kassim MB. TiO_2 doped with Fe_2O_3 for photoelectrochemical water splitting electrode: experimental and density functional theory study. Malays J Anal Sci 2016;20(4):892–900.
[10] Kay A, Grave DA, Ellis DS, Dotan H, Rothschild A. Heterogeneous doping to improve the performance of thin-film hematite photoanodes for solar water splitting. ACS Energy Lett 2016;1(4):827–33.
[11] Kobayashi R, Kurihara K, Takashima T, Ohtani B, Irie H. A silver-inserted zinc rhodium oxide and bismuth vanadium oxide heterojunction photocatalyst for overall pure-water splitting under red light. J Mater Chem 2016;4(8):3061–7.
[12] Zhang J, Ma H, Liu Z. Highly efficient photocatalyst based on all oxides WO_3/Cu_2O heterojunction for photoelectrochemical water splitting. Appl Catal B Environ 2017;201:84–91.
[13] Feng W, Lin L, Li H, Chi B, Pu J, Li J. Hydrogenated TiO_2/ZnO heterojunction nanorod arrays with enhanced performance for photoelectrochemical water splitting. Int J Hydrogen Energy 2016;42(7):3938–46.

[14] Xu Q, Qian X, Qu Y, Hang T, Zhang P, Li M, et al. Electrodeposition of Cu_2O nanostructure on 3D Cu micro-cone arrays as photocathode for photoelectrochemical water reduction. J Electrochem Soc 2016;163(10):H976–81.
[15] Lee YJ, Joo JB, Yin Y, Zaera F. Evaluation of the effective photoexcitation distances in the photocatalytic production of H_2 from water using Au@ void@ TiO_2 yolk–shell nanostructures. ACS Energy Lett 2016;1:52–6.
[16] Chen S, Thind SS, Chen A. Nanostructured materials for water splitting-state of the art and future needs: a mini-review. Electrochem Commun 2016;63:10–7.
[17] Kim H, Yong K. Highly efficient photoelectrochemical hydrogen generation using a quantum dot coupled hierarchical ZnO nanowires array. ACS Appl Mater Interfaces 2013;5(24):13258–64.
[18] Tang Y, Wang R, Yang Y, Yan D, Xiang X. Highly enhanced photoelectrochemical water oxidation efficiency based on triadic quantum dot/layered double hydroxide/$BiVO_4$ photoanodes. ACS Appl Mater Interfaces 2016;8(30):19446–55.
[19] Zhang X, Liu Y, Kang Z. 3D branched ZnO nanowire arrays decorated with plasmonic Au nanoparticles for high-performance photoelectrochemical water splitting. ACS Appl Mater Interfaces 2014;6(6):4480–9.
[20] Verma A, Srivastav A, Banerjee A, Sharma D, Sharma S, Singh UB, et al. Plasmonic layer enhanced photoelectrochemical response of Fe_2O_3 photoanodes. J Power Sources 2016;315:152–60.
[21] Verma A, Srivastav A, Sharma D, Banerjee A, Sharma S, Satsangi VR, et al. A study on the effect of low energy ion beam irradiation on Au/TiO_2 system for its application in photoelectrochemical splitting of water. Nucl Instrum Methods Phys Res Sect B Beam Interact Mater Atoms 2016;379:255–61.
[22] Kumar P, Sharma P, Solanki A, Tripathi A, Deva D, Shrivastav R, et al. Photoelectrochemical generation of hydrogen using 100 Mev Si^{8+} ion irradiated electrodeposited iron oxide thin films. Int J Hydrogen Energy 2012;37(4):3626–32.
[23] Shen S, Lindley SA, Chen X, Zhang JZ. Hematite heterostructures for photoelectrochemical water splitting: rational materials design and charge carrier dynamics. Energy Environ Sci 2016;9(9):2744–75.
[24] Tamirat AG, Rick J, Dubale AA, Su W-N, Hwang B-J. Using hematite for photoelectrochemical water splitting: a review of current progress and challenges. Nanoscale Horizons 2016;1:243–67.
[25] Malviya KD, Dotan H, Shlenkevich D, Tsyganok A, Mor H, Rothschild A. Systematic comparison of different dopants in thin film hematite (α-Fe_2O_3) photoanodes for solar water splitting. J Mater Chem 2016;4(8):3091–9.
[26] Luo J, Steier L, Son M-K, Schreier M, Mayer MT, Grätzel M. Cu_2O nanowire photocathodes for efficient and durable solar water splitting. Nano Lett 2016;16(3):1848–57.
[27] Qi H, Wolfe J, Fichou D, Chen Z. Cu_2O photocathode for low bias photoelectrochemical water splitting enabled by NiFe-layered double hydroxide Co-catalyst. Sci Rep 2016;6.
[28] Cheng Y, Memar A, Saunders M, Pan J, Liu C, Gale JD, et al. Dye functionalized carbon nanotubes for photoelectrochemical water splitting–role of inner tubes. J Mater Chem 2016;4(7):2473–83.
[29] Li MMJ, Mills P, Fairclough SM, Robertson A, Peng Y-K, Warner J, et al. Importance of the structural integrity of a carbon conjugated mediator for photocatalytic hydrogen generation from water over a CdS-carbon nanotube-MoS_2 composite. Chem Commun 2016;52(93):13596–9.
[30] Das D, Nanda KK. One-step, integrated fabrication of Co 2 P nanoparticles encapsulated N, P dual-doped CNTs for highly advanced total water splitting. Nano Energy 2016;30:303–11.
[31] Kongkanand A, Martínez Domínguez R, Kamat PV. Single wall carbon nanotube scaffolds for photoelectrochemical solar cells. Capture and transport of photogenerated electrons. Nano Lett 2007;7(3):676–80.
[32] Li DJ, Maiti UN, Lim J, Choi DS, Lee WJ, Oh Y, et al. Molybdenum sulfide/N-doped CNT forest hybrid catalysts for high-performance hydrogen evolution reaction. Nano Lett 2014;14(3):1228–33.
[33] Park J, Choi W. TiO_2- nafion photoelectrode hybridized with carbon nanotubes for sensitized photochemical activity. J Phys Chem C 2009;113(49):20974–9.
[34] Kongkanand A, Kamat PV. Electron storage in single wall carbon nanotubes. Fermi level equilibration in semiconductor–SWCNT suspensions. ACS Nano 2007;1(1):13–21.
[35] Kecsenovity E, Endr}odi B, Papa Z, Hernadi K, Rajeshwar K, Janaky C. Decoration of ultra-long carbon nanotubes with Cu_2O nanocrystals: a hybrid platform for enhanced photoelectrochemical CO_2 reduction. J Mater Chem A 2016:1–9.
[36] Chaudhary D, Singh S, Vankar V, Khare N. A ternary Ag/TiO_2/CNT photoanode for efficient photoelectrochemical water splitting under visible light irradiation. Int J Hydrogen Energy 2017;42:7826–35.
[37] Wang N, Li J, Wu L, Li X, Shu J. MnO_2 and carbon nanotube co-modified C_3N_4 composite catalyst for enhanced water splitting activity under visible light irradiation. Int J Hydrogen Energy 2016;41:22743–50.
[38] Song L, Kang X, Zhang S. CNT/g-C_3N_4 photocatalysts with enhanced hydrogen evolution ability for water splitting based on a noncovalent interaction. Int J Energy Res 2018:1–8.
[39] Chaudhary D, Singh S, Vankar V, Khare N. ZnO nanoparticles decorated multi-walled carbon nanotubes for enhanced photocatalytic and photoelectrochemical water splitting. J Photochem Photobiol Chem A 2018;351:154–61.
[40] Kim JY, Jang J-W, Youn DH, Kim JY, Kim ES, Lee JS. Graphene–carbon nanotube composite as an effective conducting scaffold to enhance the photoelectrochemical water oxidation activity of a hematite film. RSC Adv 2012;2(25):9415–22.
[41] Kim JY, Jun H, Hong SJ, Kim HG, Lee JS. Charge transfer in iron oxide photoanode modified with carbon nanotubes for photoelectrochemical water oxidation: an electrochemical impedance study. Int J Hydrogen Energy 2011;36(16):9462–8.
[42] Liu Y, Wang D-P, Yu Y-X, Zhang W-D. Preparation and photoelectrochemical properties of functional carbon nanotubes and Ti co-doped Fe_2O_3 thin films. Int J Hydrogen Energy 2012;37(12):9566–75.
[43] Pawar RC, Choi D-H, Lee CS. Reduced graphene oxide composites with MWCNTs and single crystalline hematite nanorhombohedra for applications in water purification. Int J Hydrogen Energy 2015;40(1):767–78.
[44] Li C, Wang J, Jiang Z, Hu P. Co/Cu_2O assisted growth of graphene oxide on carbon nanotubes and its water splitting activities. N J Chem 2015;39(6):4562–7.
[45] Wang J-C, Zhang L, Fang W-X, Ren J, Li Y-Y, Yao H-C, et al. Enhanced photoreduction CO_2 activity over direct Z-scheme α-Fe_2O_3/Cu_2O heterostructures under visible light irradiation. ACS Appl Mater Interfaces 2015;7(16):8631–9.
[46] Sharma D, Upadhyay S, Verma A, Satsangi VR, Shrivastav R, Dass S. Nanostructured Ti-Fe_2O_3/Cu_2O heterojunction photoelectrode for efficient hydrogen production. Thin Solid Films 2015;574:125–31.
[47] Wang J, Du C, Peng Q, Yang J, Wen Y, Shan B, et al. Enhanced photoelectrochemical water splitting performance of hematite nanorods by Co and Sn co-doping. Int J Hydrogen Energy 2017;42:29140–9.

[48] Li L, Liu C, Qiu Y, Mitsuzak N, Chen Z. Convex-nanorods of α-Fe_2O_3/CQDs heterojunction photoanode synthesized by a facile hydrothermal method for highly efficient water oxidation. Int J Hydrogen Energy 2017;42:19654–63.
[49] Zhang Q, Wang H, Dong Y, Wu Q, Xue S. Highly efficient hematite films via mid-/ex-situ Sn-doping for photoelectrochemical water oxidation. Int J Hydrogen Energy 2017;42:16012–22.
[50] Chen H-L, Chiang T-H, Wu M-C. Evolution of morphology of nano-scale CuO grown on copper metal sheets in 5 wt% NaCl solution of spray fog environment. J Surf Eng Mater Adv Technol 2012;2(04):278.
[51] Su JF, Ruzybayev I, Shah I, Huang C. The electrochemical reduction of nitrate over micro-architectured metal electrodes with stainless steel scaffold. Appl Catal B Environ 2016;180:199–209.
[52] Gonçalves RH, Leite ER. The colloidal nanocrystal deposition process: an advanced method to prepare high performance hematite photoanodes for water splitting. Energy Environ Sci 2014;7(7):2250–4.
[53] Srivastav A, Verma A, Banerjee A, Khan SA, Gupta M, Satsangi VR, et al. Gradient doping–a case study with Ti-Fe_2O_3 towards an improved photoelectrochemical response. Phys Chem Chem Phys 2016;18(48):32735–43.
[54] Chan GH, Zhao J, Hicks EM, Schatz GC, Van Duyne RP. Plasmonic properties of copper nanoparticles fabricated by nanosphere lithography. Nano Lett 2007;7:1947–52.
[55] Li Y, Yu H, Zhang C, Fu L, Li G, Shao Z, et al. Enhancement of photoelectrochemical response by Au modified in TiO_2 nanorods. Int J Hydrogen Energy 2013;38:13023–30.
[56] Shen H, Liu G, Yan X, Jiang J, Hong Y, Yan M, et al. All-solid-state Z-scheme system of RGO-Cu_2O/Fe_2O_3 for simultaneous hydrogen production and tetracycline degradation. Mater Today Energy 2017;5:312–9.